

Spatial multiomics of acute myocardial infarction reveals immune cell infiltration through the endocardium

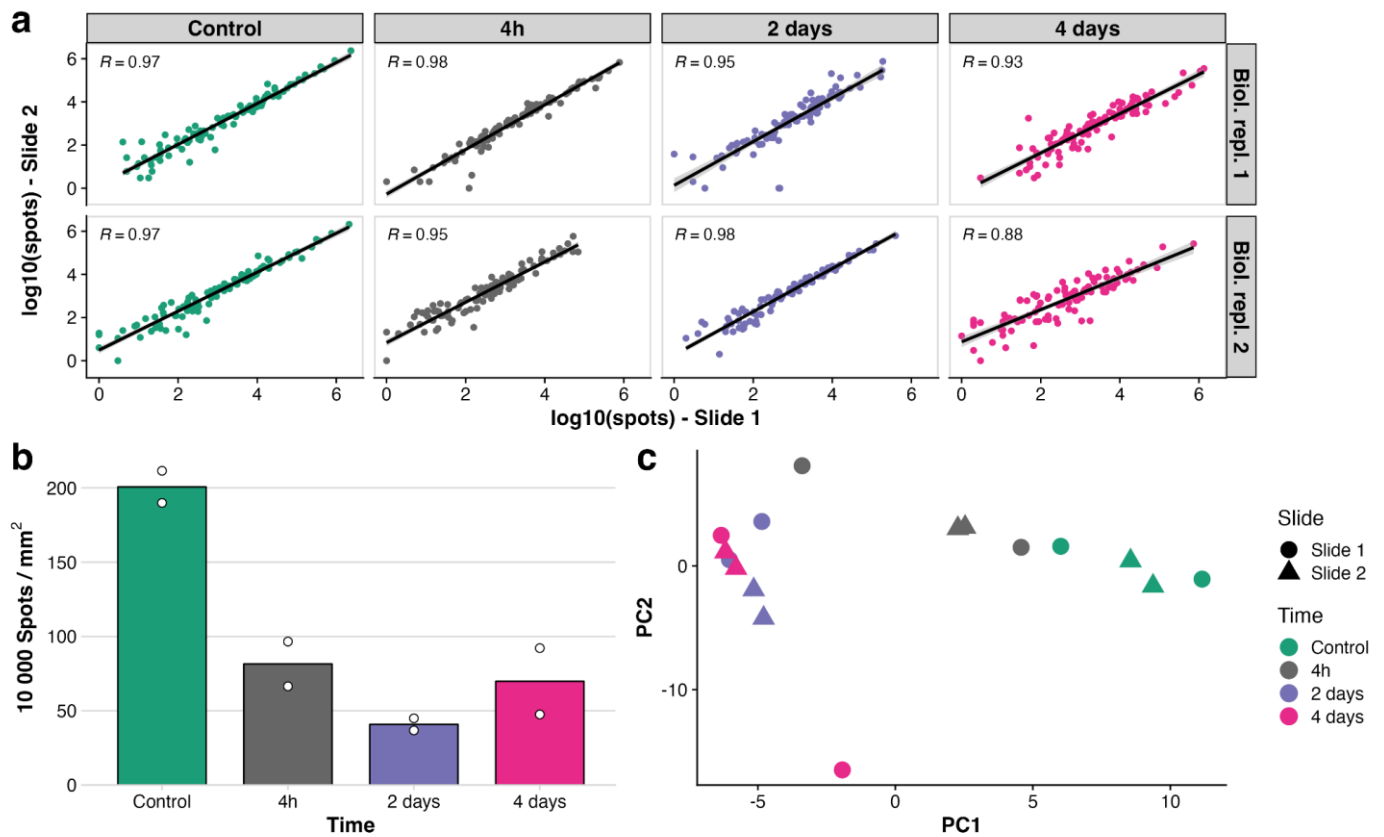
In the format provided by the
authors and unedited

Table of Contents - Supplementary Information

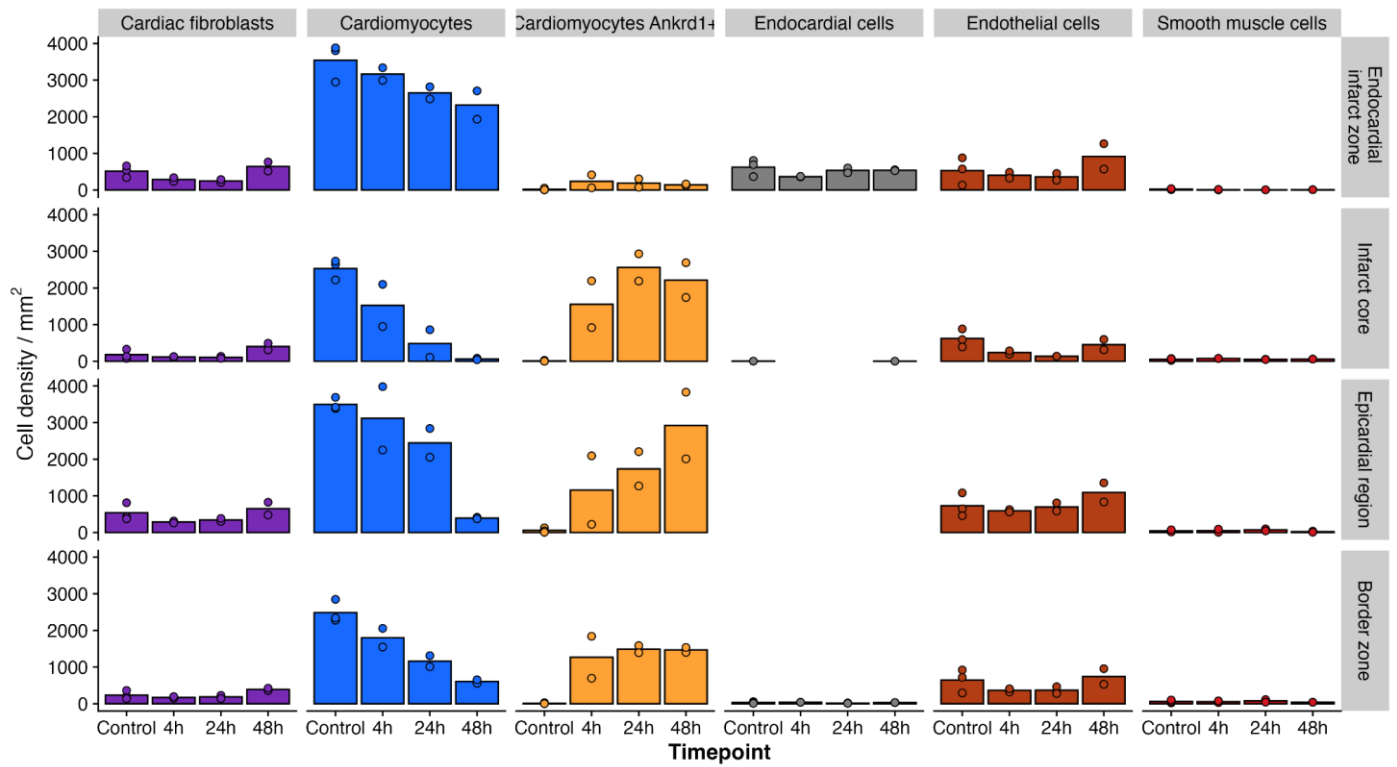
Supplementary Figures

Supplementary Figure 1
Supplementary Figure 2
Supplementary Figure 3
Supplementary Figure 4
Supplementary Figure 5
Supplementary Figure 6
Supplementary Figure 7
Supplementary Figure 8
Supplementary Figure 9
Supplementary Figure 10

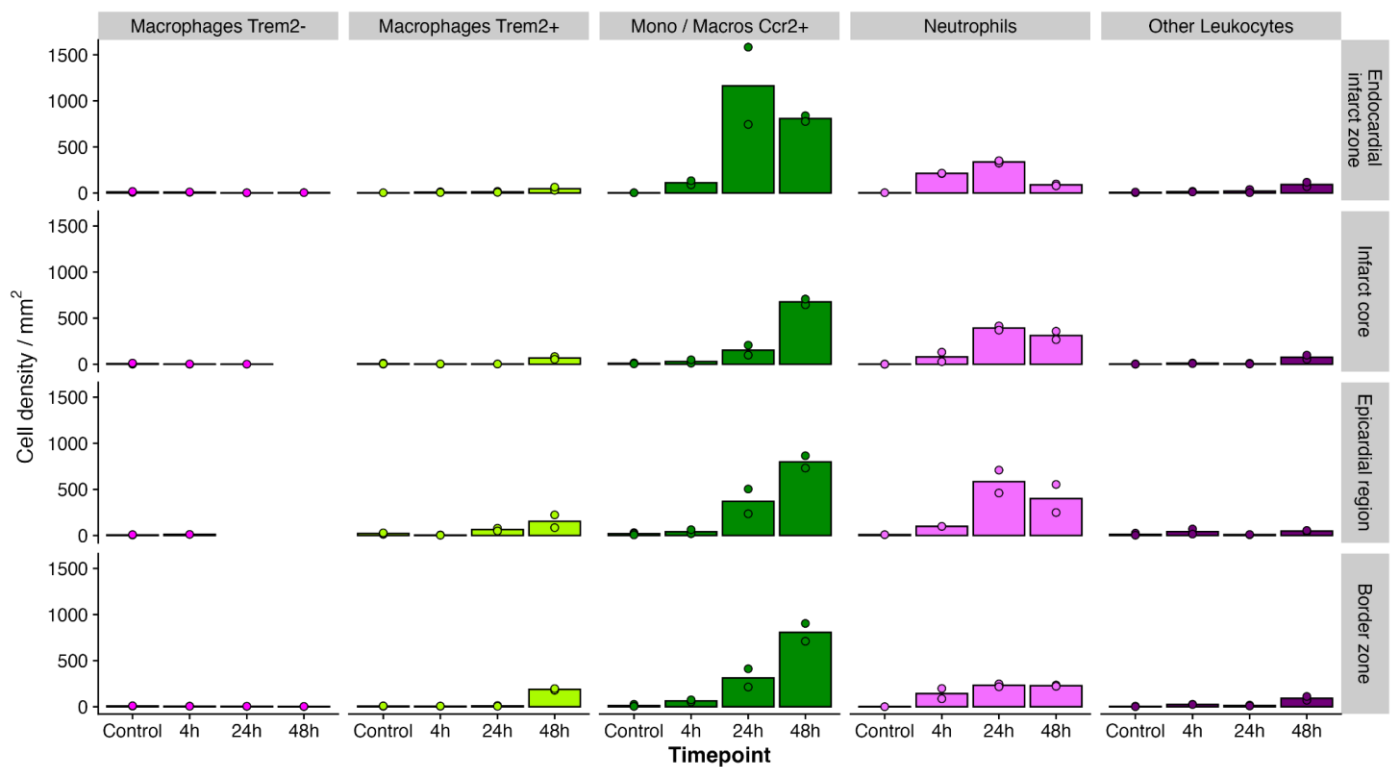
Supplementary Figures



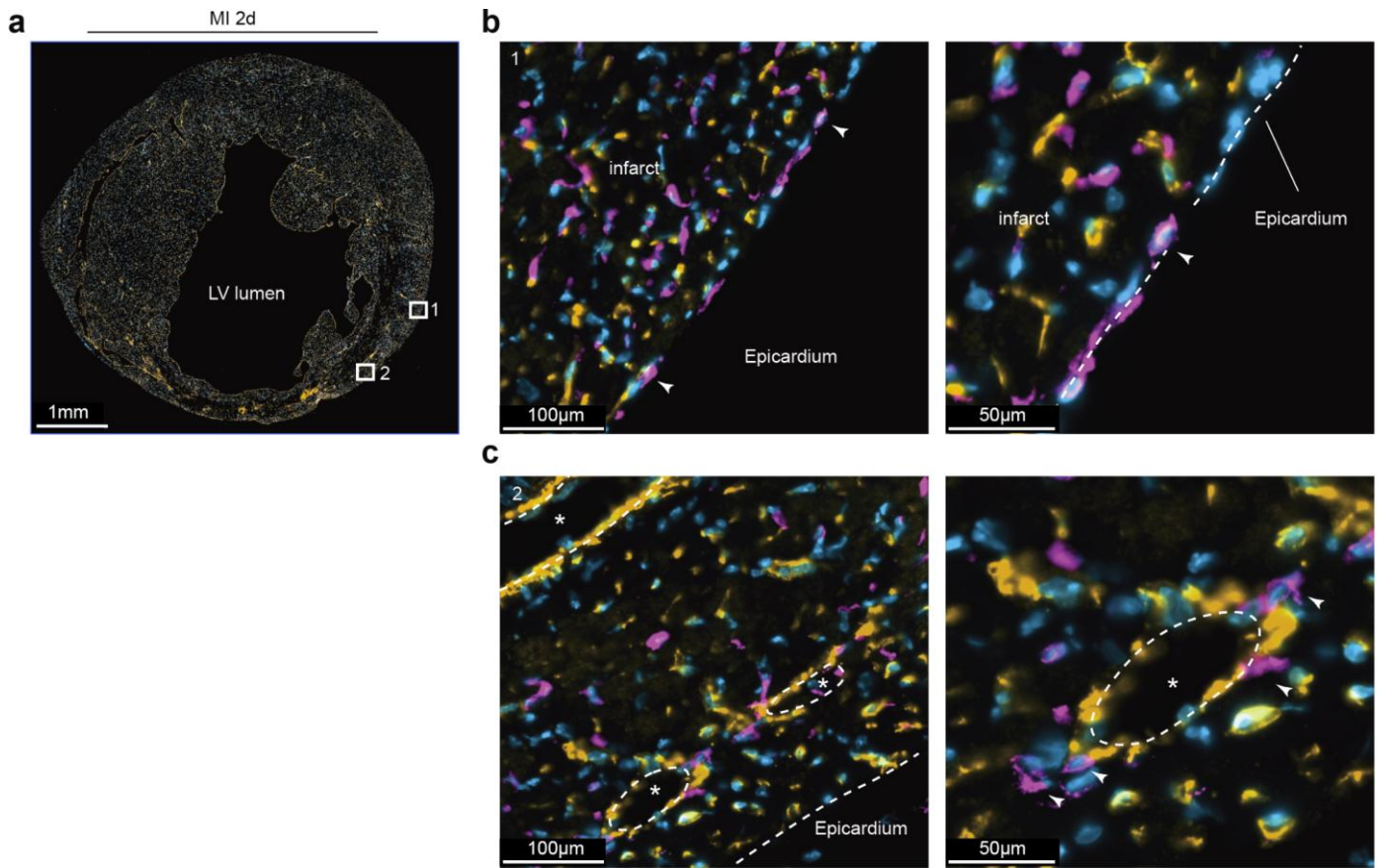
Supplementary Figure 1: Quality control of Molecular Cartography RNA spot count data. **a)** Correlation between technical replicates across two runs of Molecular Cartography across four timepoints of acute MI. R: Pearson correlation coefficient of log10 spot sum between technical replicates. **b)** Relative number of RNA spots identified per square micrometre of tissue measured using Molecular Cartography. **c)** Principal component analysis of samples by total RNA spots per gene. The outlier samples for the 4-hour and 4-day time points both have multiple small image tiles with spots missing due to failing quality control during spot calling by Resolve Bioscience.



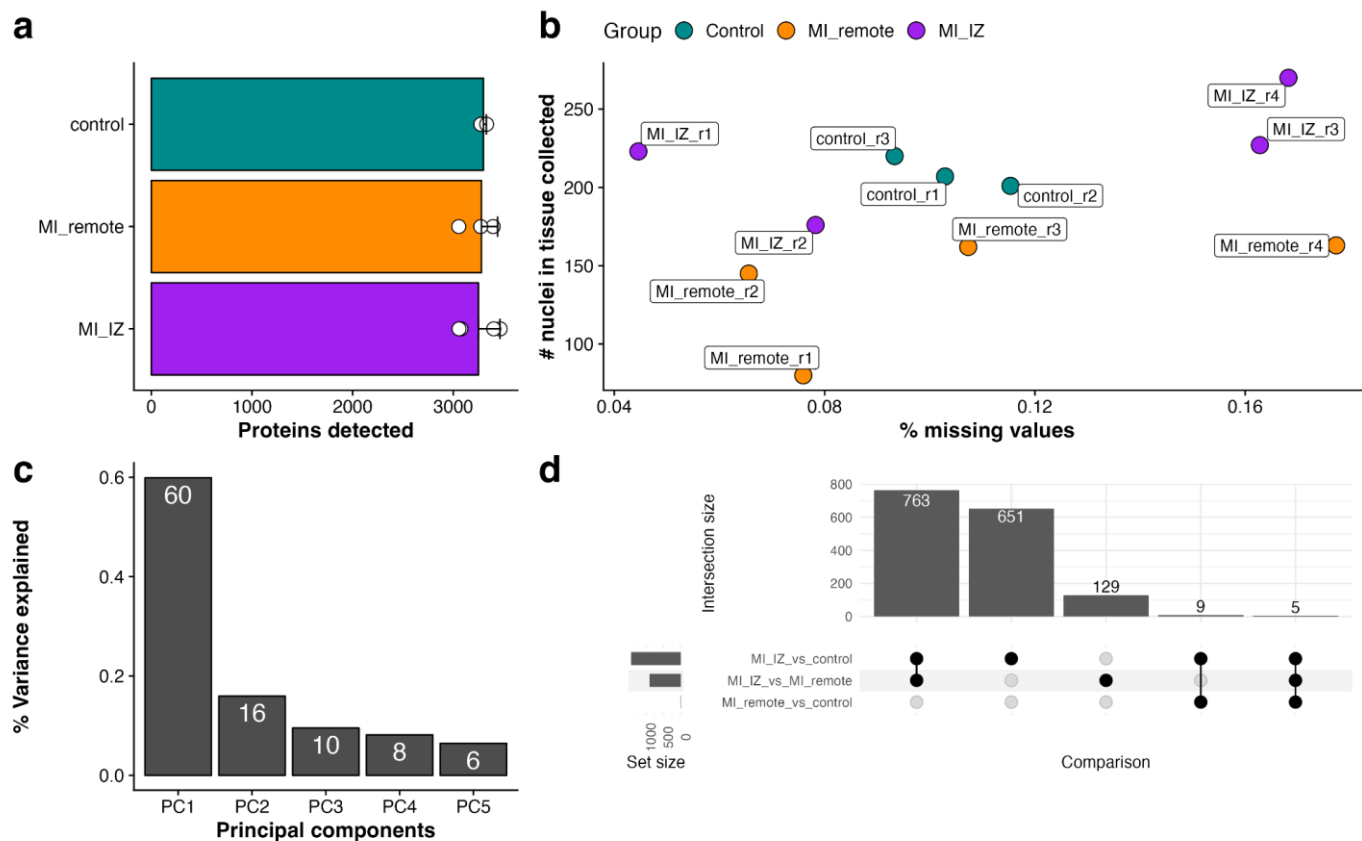
Supplementary Figure 2: Density of non-immune cells in different regions of the heart across acute MI in SeqIF data. Bars represent mean cell density across biological replicates and points represent individual measurements (n= 3 for control, n=2 for infarct groups).



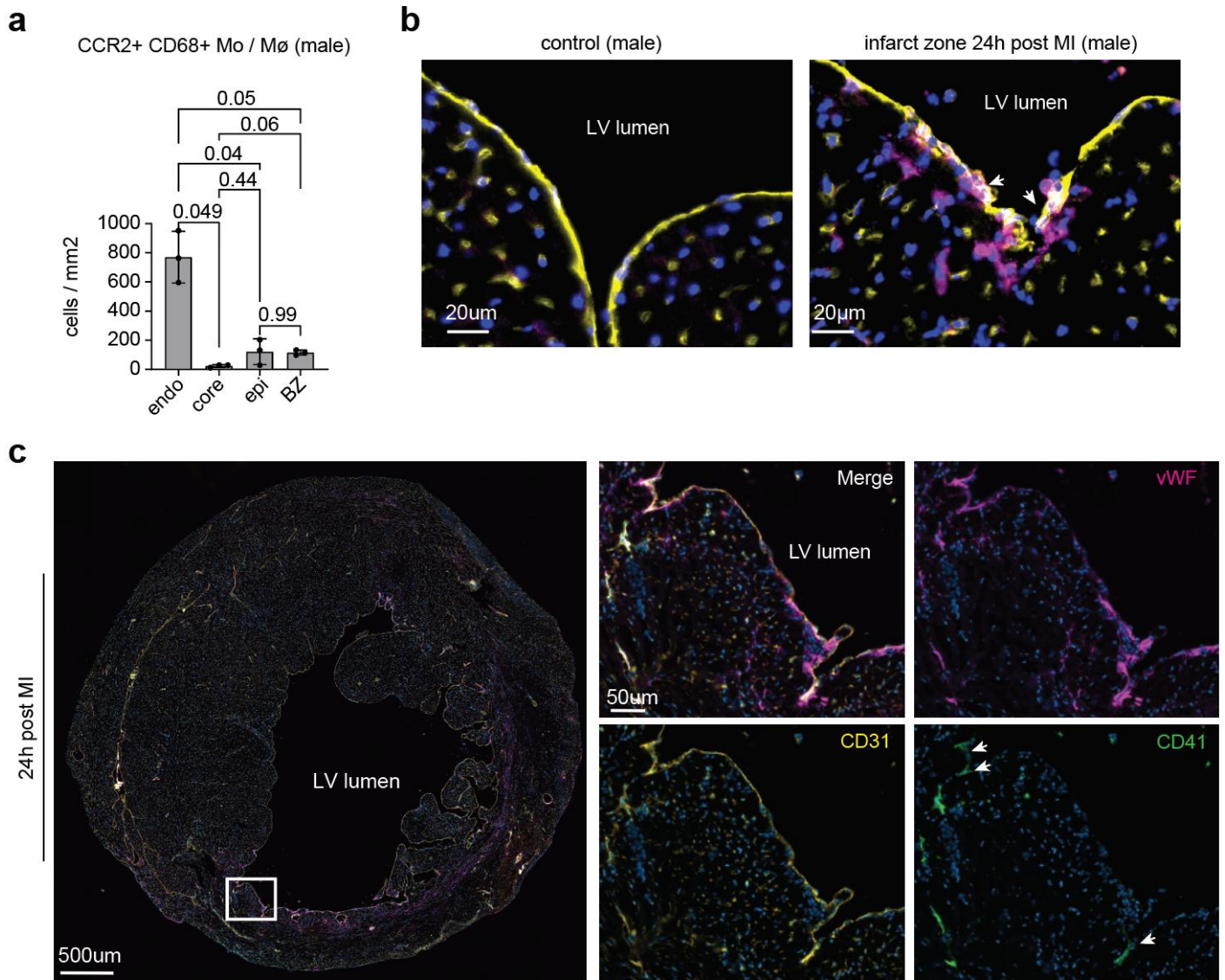
Supplementary Figure 3: Density of immune cells in different regions of the heart across acute MI in SeqIF data. Bars represent mean cell density across biological replicates and points represent individual measurements (n= 3 for control, n=2 for infarct groups).



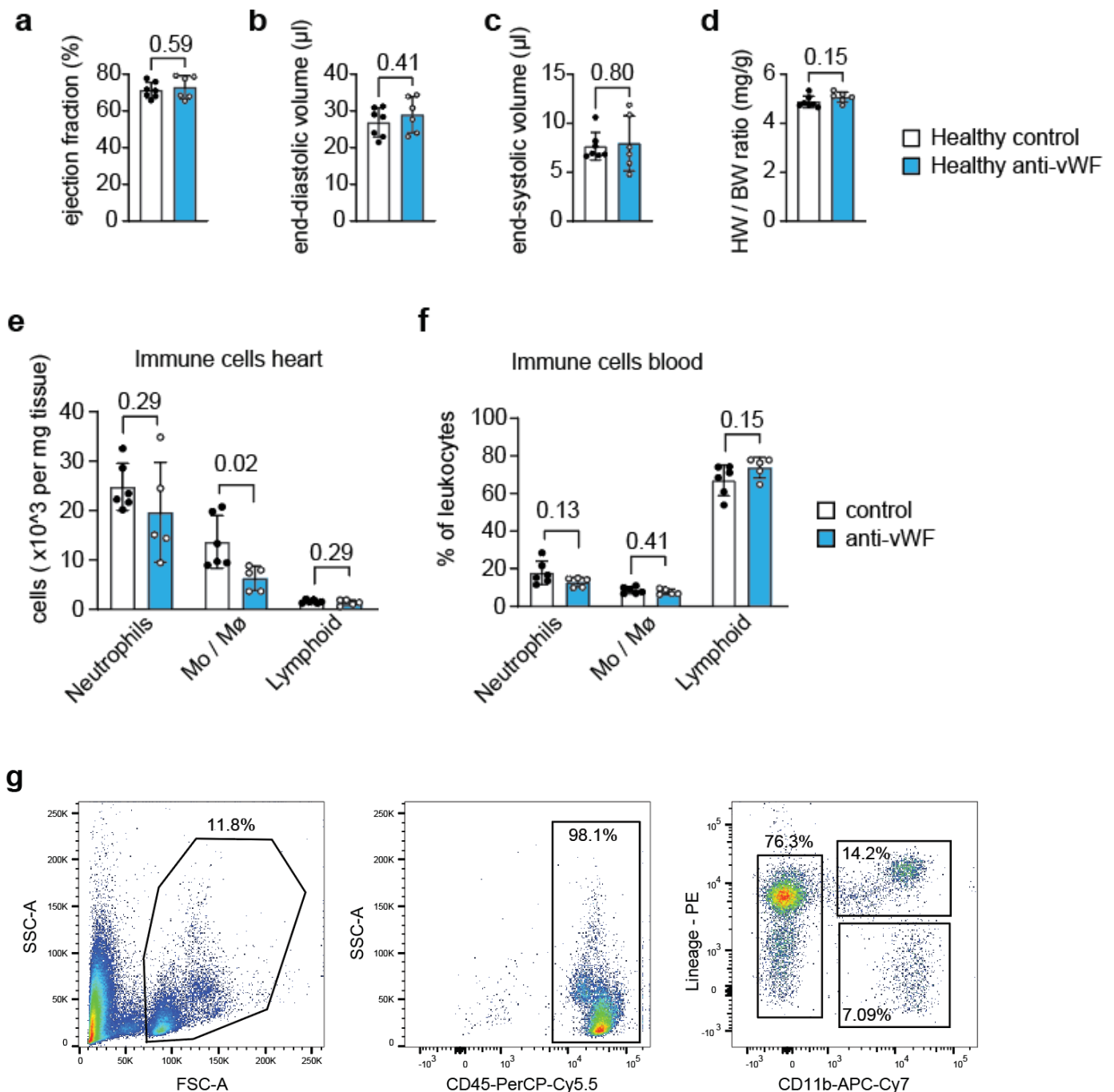
Supplementary Figure 4: CCR2+ cells in proximity to epicardium and epicardial vessels. a) Overview section 2d post-MI with staining of CD31 (yellow), CCR2 (magenta) and DAPI (blue). b) and c) Magnified areas with a focus on the epicardial region displaying CCR2+ cells on the surface of the epicardium (arrows) and epicardial vessels (marked by asterisks). The mid and right panel displays magnifications of the marked box in the left overview panel.



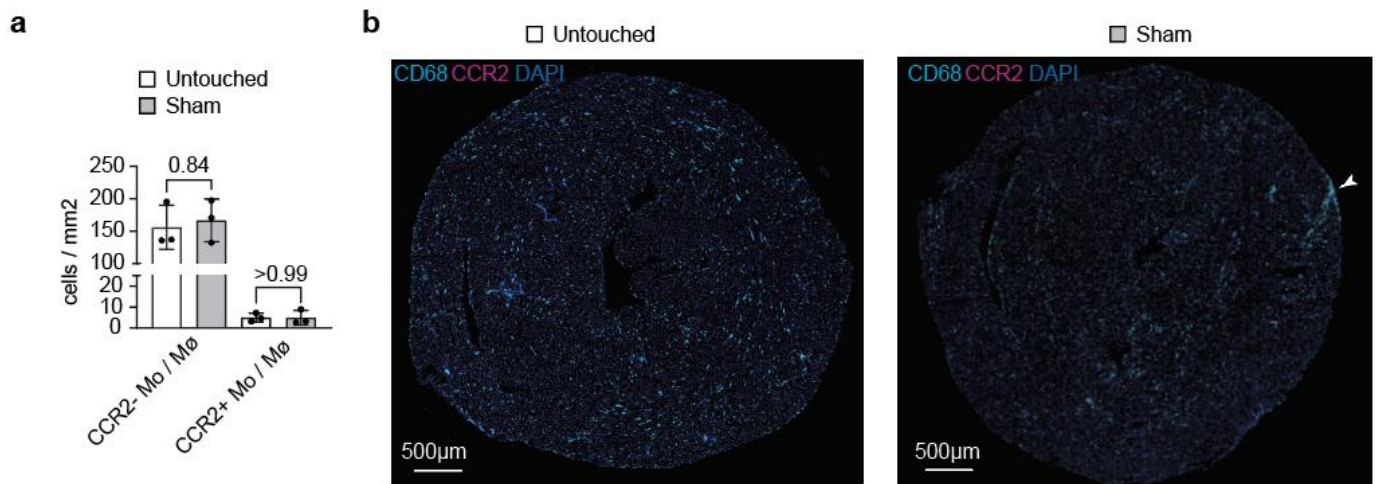
Supplementary Figure 5: Quality control of DVP data. a) Number of proteins identified per sample within each treatment / subregion group. **b)** Scatterplot showing the percentage of missing values in the proteomic data against the number of nuclei that were detected within the region marked for laser microdissection **c)** Percent variance explained by the first five principal components for proteomics data. Principal component one separates samples by treatment group / subregion and explains 60% of the variance within the data. **d)** Upset plot showing overlap between significantly differentially expressed proteins between all three laser microdissected regions.



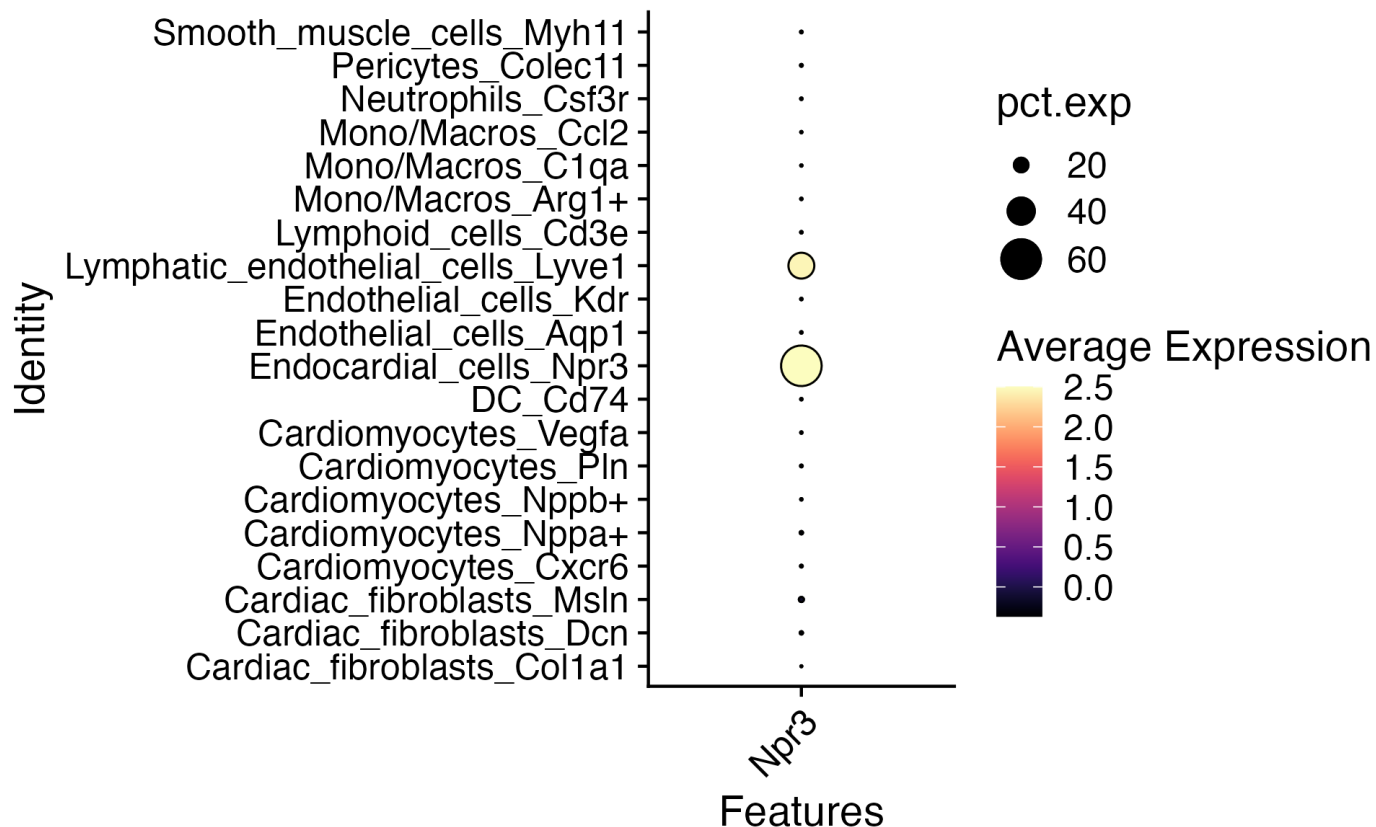
Supplementary Figure 6: a) Quantification of infiltrating CCR2+ CD68+ Mo/M ϕ in different regions of the infarcted heart 24 hours post-MI in male mice. Data show mean \pm SD (n=3 per group). *P* values were determined by one-way ANOVA with repeated measurements followed by Tukey multiple comparison. **b)** Representative immunofluorescence stainings of CCR2+ cells (magenta) in the healthy and infarcted myocardium of male mice. DAPI in blue and CD31 in yellow. Arrows indicate CCR2+ attaching or infiltrating at the endocardial layer. **c)** Co-staining of vWF, CD31 and CD41 in the infarct region 24h after permanent occlusion indicates a platelet-independent mechanism. Arrows indicate CD41+ platelets in some but not all vWF+ areas.



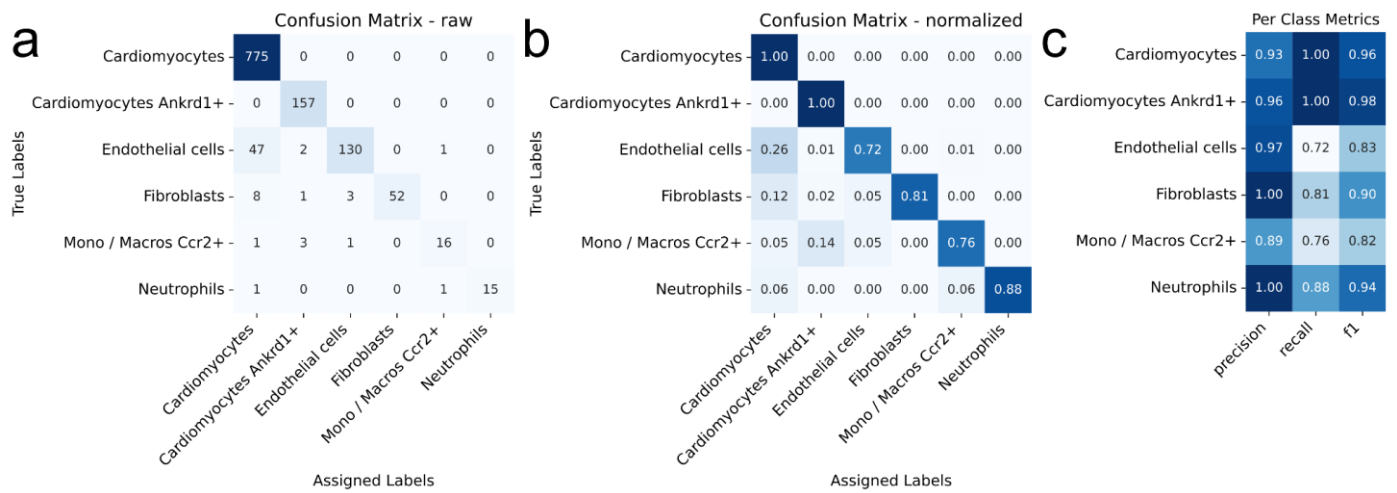
Supplementary Figure 7: Effects of anti-vWF blockade via antibody in healthy and infarcted mice. a-c) LV ejection fraction, end-systolic and end-diastolic volume determined by echocardiography 14d after antibody treatment in healthy mice (n=7 for control, n=6 for anti-vWF). *P* value was calculated using 2-tailed Student t test. **d)** Heart weight to body weight ratios after organ removal. **e)** Absolute counts of neutrophils, Mo/Mφ and lymphoid cell based on flow cytometry analysis of digested heart at the 2 day post-MI time point in anti-vWF treated mice (n=5) compared to controls (n=6). *P* values were calculated using 2-tailed Student t test. **f)** Relative cell counts (in % of total blood leukocytes) 2 days post-MI in anti-vWF treated and the control mice. *P* values were calculated using 2-tailed Student t test. **g)** Gating strategy for quantification of blood cell counts. Mo/Mφ were identified as CD45+, Lin-(CD19;CD4;NK1.1;Ly6G;Ter119), CD11b+. Neutrophils were identified as CD45+, Lin+(CD19;CD4;NK1.1;Ly6G;Ter119), CD11b+. Lymphoid cells were gated CD45+, Lin-(CD19;CD4;NK1.1;Ly6G;Ter119), CD11b-.



Supplementary Figure 8: Monocyte / macrophage counts in untouched and sham-operated mice. a) Quantification of CCR2+ CD68+ and CCR2- CD68+ Mo/Mφ in untouched and sham-operated hearts (24 hours after sham intervention). Data show mean±SD (n=3 per group). *P* values were calculated using 2-tailed Student *t* test. **b)** Co-staining of CCR2, CD68 and DAPI in hearts of untouched and sham-operated mice. The arrow marks a lesion with defined accumulation of CD68+ Mo/Mφ caused by electrocoagulation.



Supplementary Figure 9: Dotplot showing Npr3 expression over fine-grained cell type annotations in the Molecular Cartography dataset. While Npr3 is primarily expressed in the Endocardial cells in our data set, the absence of detected Npr3 transcripts in a subset of endocardial cells may reflect transcriptional heterogeneity and/or technical limitations of Molecular Cartography in capturing low-abundance transcripts.



Supplementary Figure 10: Evaluation of Pixie-based phenotyping by comparison to an independently labeled ground truth data subset focusing on phenotypes which appear 10 or more times in the corresponding annotations. a) Confusion matrix containing the absolute number of assertions for each pair of true and assigned labels. **b)** Normalized confusion matrix containing the scaled assertions for each true class. **c)** Summary of precision, recall and F1 scores for each phenotype.